Journal of Materials Chemistry B

ROYAL SOCIETY OF CHEMISTRY

PAPER

View Article Online
View Journal | View Issue

Check for updates

Cite this: J. Mater. Chem. B, 2025, 13, 5109

Flavin-based probe for real-time monitoring of hypochlorous acid dynamics in live cells†

Harsha Gopal Agrawal,[a] Pravin Shankar Giri,[b] Tanima Sahoo,[a] Subha Narayan Rath *[b] and Ashutosh Kumar Mishra *[a]

Received 8th December 2024, Accepted 24th March 2025

DOI: 10.1039/d4tb02727b

rsc.li/materials-b

The present study introduces TPA-vinylene-flavin (**TVF**) as a flavin-based turn-on fluorescent probe. **TVF** effectively detects HOCl, as evaluated by the solution phase studies with a detection limit of 0.36 μM. This probe shows excellent biocompatibility and rapid cellular internalization, making it suitable for real-time monitoring of HOCl fluctuations in both physiological and pathological conditions. Furthermore, the **TVF** probe exhibits specific mitochondrial localization and selectively detects HOCl in both endogenous and exogenous contexts within live cells. It demonstrates excellent sensitivity to HOCl concentrations over time, enabling precise tracking of dynamic fluctuations, which is critical for understanding its role in cellular processes and oxidative stress-related pathologies.

Introduction

Recent advancements in science and technology have revolutionized the field of diagnostics through interventions of newer technologies in detecting biomarkers in the subcellular spaces. Substantial evidence indicates that various bioactive molecules play a crucial role in regulating physiological processes throughout the cell cycle, and their abnormal expression is linked to several major diseases.[1] Also, the concentrations of these molecules vary across different subcellular organelles and are dependent on the existing physiological conditions. Hence, accurately detecting the presence of these molecules at an organelle level can enhance our knowledge regarding the prevailing physiological and pathological processes.[2]

Considerable efforts have been directed towards the design and development of organelle-targeted fluorescent probes for the precise monitoring of subcellular microenvironments, such as pH,[3–5] polarity,[6] ions,[7,8] viscosity.[9,10] reactive oxygen species (ROS),[11,12] reactive nitrogen species (RNS),[12,13] and reactive sulfur species (RSS).[14–16] Among these targets, ROS, RNS, and RSS—collectively termed RONSS[1]—have garnered increasing attention due to their critical role in intracellular redox homeostasis.

Among all these ROS, hypochlorous acid is one of the highly reactive species, and fluctuations in its production indicate the functional status of cells.[17] Physiologically, HOCl is produced by a reaction between H_2O_2 and chloride ions mediated by a class of enzymes, myeloperoxidases (MPO).[18,19]

HOCl plays an essential role in defence against deadly pathogens due to its high bactericidal and oxidative activity compared to other species.[20,21] Endogenously, HOCl is produced by various immune cells, including neutrophils, monocytes, macrophages, and even some cancer cells. However, elevated HOCl production can trigger significant damage to cellular organelles, including mitochondria,[22] potentially leading to various diseases such as cancer,[23] arthritis,[2] neurodegenerative disorders,[24] liver damage,[25] and other conditions.[26,27] Hence, various methods to trace significant changes in biological HOCl with high oxidative activity in real-time are crucial for cellular and tissue imaging and early disease prevention.

In this context, significant advancements have been made in developing probes for HOCl detection, including probes built around derivatives of BODIPY, coumarin, triphenylamine, Nile Red, naphthalene imide, and rhodamine displaying excellent biocompatibility and selectivity.[22,26–30] However, despite their advantages, many of these probes suffer from drawbacks such as potential interference from other ROS, and challenges in achieving precise organelle targeting. These limitations have driven the search for alternative fluorophores with improved performance in complex biological environments.

Now, flavin-based derivatives, as fluorescent probes, have spurred interest, particularly for detecting reactive oxygen species.[31] Building on our ongoing work in developing novel flavin-based designs for various applications,[32–41] we have recently reported a TPA-flavin probe that enables effective fluorescent labelling of mitochondria and real-time monitoring of dynamic microenvironments, especially under hypoxic conditions.[42] This probe offers advantages such as exceptional

[a] Department of Chemistry, Indian Institute of Technology Hyderabad, Kandi, 502284, Telangana, India. E-mail: akm@chy.iith.ac.in
[b] Department of Biomedical Engineering, Indian Institute of Technology Hyderabad, Kandi, 502284, Telangana, India

† Electronic supplementary information (ESI) available. See DOI: https://doi.org/10.1039/d4tb02727b

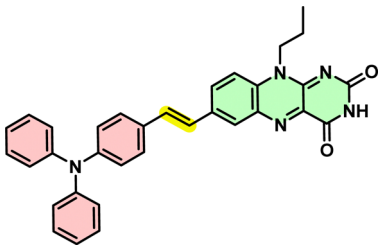

Scheme 1 Design of TPA-based molecular rotor Triphenylamine-vinylene-flavin (**TVF**).

biocompatibility, rapid cellular internalization, and stability within cellular environments.[42] Based on this approach, we have designed and synthesized a TPA-vinylene-flavin (**TVF**, Scheme 1) probe, incorporating an alkene functionality between TPA and Flavin. This structural modification can enhance the specificity of the probe toward hypochlorous acid, given that the double bond is susceptible to oxidative addition.[43] The **TVF** probe exhibits high selectivity and enhanced sensitivity for HOCl detection among other ROS species with a detection limit of 0.36 μM. Furthermore, we have investigated cytocompatibility, tracking cellular HOCl and specific organelle localization to evaluate its potential for biosensing applications.

Results and discussion

The **TVF** probe was synthesized in a simple four-step synthetic protocol, as shown in Scheme 2. Briefly, the *n*-propyl chain was introduced, by nucleophilic aromatic substitution (S_NAr) reaction using *n*-propyl amine and fluoro-2-nitrobenzene derivative to give substituted nitro-amine derivative **1**. Further, alkene functionality was introduced onto triphenylamine through a Wittig reagent and an aldehyde to give compound **2**. Afterward, the substituted nitro-amine **1** derivative and compound **2** undergoes, the palladium-catalysed Heck coupling reaction to give vinylene triphenylamine linked nitro compound **3**. Subsequently, compound **3** undergoes the reduction of the nitro group into diamine by catalytic hydrogenation followed by treatment with alloxan monohydrate in the presence of boric acid to get the target molecule **TVF**. All the compounds were characterized using ^{1}H NMR, ^{13}C NMR, and ESI-HRMS spectroscopy, and corresponding spectra are provided in ESI.†

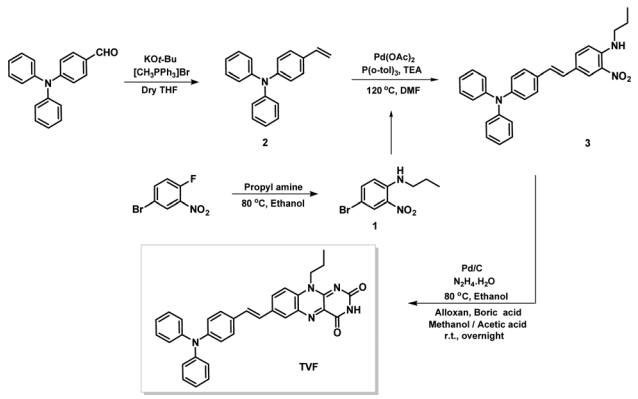

Scheme 2 Synthesis of TPA-vinylene-flavin (**TVF**).

The optical properties were investigated to understand the luminescence characteristics associated with **TVF**. As depicted in Fig. S1 (ESI†), an absorption study carried out in methanol solvent unveils a pronounced absorption band at 380 nm, along with broadband that is evident in the longer wavelength region, particularly at λ_{max} 509 nm (Fig. S1, ESI†). In comparison to the parent flavin moiety (N10-propyl isoalloxazine, **PFl**, which is devoid of any substitution at the C7 position), exhibits absorption maxima at 330 and 435 nm, there is notable bathochromic shift exists for **TVF**, thereby implying an overlapping contribution from the TPA-vinylene group to the flavin. Moreover, to systematically assess the influence of the solvent medium on the optical properties of **TVF**, both the absorption and emission spectra were recorded in various solvents (Fig. 1), and a comprehensive set of photophysical parameters are summarized in Tables S1 and S2 (ESI†).

In absorption spectra with different solvent polarities, although a significant change was observed in the absorption maxima, it does not follow a simple correlation with the increasing polarity of the solvent. To further understand the solvent effect of the probe, emission spectra of the **TVF** were recorded, as shown in Fig. 1b. A strong emission band was observed, particularly in nonpolar solvents like toluene and dioxane, exhibiting a blue shift of ~20 nm in dioxane relative to toluene. However, the total quenching of the emission spectra was recorded in the remaining solvents. The observed variation from non-polar to polar solvent in the emission spectra can likely be attributed to differences in the degree of solute–solvent interactions in the excited state, which in turn affects the efficiency of the charge transfer process.

To investigate the susceptibility of the double bond in **TVF** for oxidative response, we examined its fluorescence behavior upon the addition of HOCl. The fluorescence spectra were recorded with increasing concentrations of NaOCl (0–6 equivalents) as the source of HOCl at two different excitation wavelengths. The selection of these two excitation wavelengths was based on the distinct absorption maxima of **TVF** and its control molecule, PFl. **TVF** absorbs at 511 nm wavelength, while PFl, which lacks the vinylene-TPA moiety, absorbs at 435 nm. By exciting at both wavelengths, we aimed to determine whether the fluorescence originated from an intact **TVF** probe or if it resulted from its oxidative breakdown upon reaction with HOCl.

At an excitation wavelength of 511 nm (the absorption maximum of **TVF** in methanol), the addition of NaOCl resulted

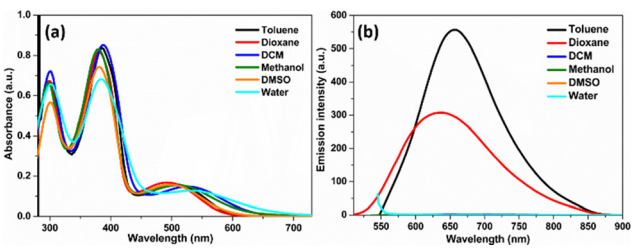

Fig. 1 (a) UV-visible and (b) fluorescence spectra of **TVF** in different solvents at 19 μM concentration.

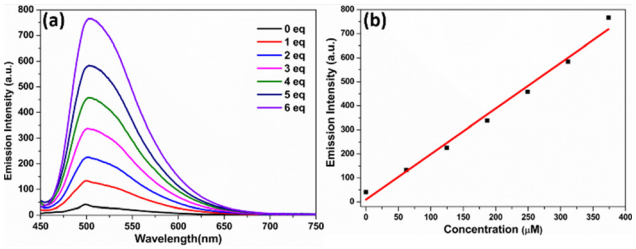

Fig. 2 (a) Fluorescence spectra of **TVF** (62 μM) with the addition of different concentrations of NaOCl (0–6 eq.) in methanol. λ_{ex} = 435 nm. (b) The fluorescence intensities at 507 nm *vs.* increasing concentrations of HOCl. Each spectrum was acquired 5 min after HOCl addition.

in no detectable emission in the 600–800 nm range (Fig. S4, ESI†). Conversely, when excited at 435 nm (the absorption maximum of the control molecule, PFl, which lacks the vinylene-TPA moiety, Fig. S1, ESI†), the fluorescence intensity at 507 nm increased progressively with the addition of NaOCl (Fig. 2a). This observation suggests the possibility of oxidative breakdown of **TVF**. A linear relationship was observed between the fluorescence intensity of **TVF** at 507 nm and the concentration of HOCl (0–500 μM), with a detection limit calculated as 0.36 μM based on the $3\sigma/s$ method (Fig. 2b). Notably, **TVF** exhibited negligible fluorescence in methanol with a fluorescent quantum yield of 0.007. However, upon addition of 1 equivalent of NaOCl, the fluorescence intensity at 507 nm was observed to increase significantly, corresponding to a fluorescence quantum yield of 0.01 (using Rhodamine 6G in ethanol as the standard), thereby confirming the role of the **TVF** probe in sensing HOCl.

To evaluate the specificity of the **TVF** probe, we have used TPA-flavin molecule as control, which lacks the double bond between the TPA and Flavin moiety. Upon the addition of 10 equivalents of HOCl, no significant increase in fluorescence intensity was observed, confirming the involvement of the double bond for the oxidative response (Fig. S5, ESI†).

To have an insight into the possible detection mechanism of the ClO^- species by **TVF** moiety (Scheme 3), the HRMS analysis of the crude reaction mixture containing the **TVF** and NaOCl was recorded and is shown in Fig. S6 (ESI†). The ESI-MS (+mode) spectra reveal a dominant peak at m/z = 542.2164 (cal. 542.2192), corresponding to the epoxy-**TVF** intermediate formation because of oxidation of the double bond by the ClO^- species. Further, oxidative degradation of the epoxy-**TVF** intermediate results in peaks corresponding to TPA-aldehyde, as evidenced by the peak at m/z = 274.1217 (cal. 274.1232) (Fig. S6b, ESI†). Based on these observed, it is proposed that the spectral changes observed in the presence of NaOCl possibly originated from the oxidative cleavage of **TVF**, proceeding through an epoxide intermediate before yielding the other by-products.

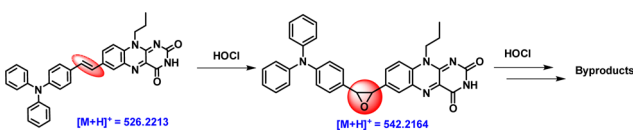

Scheme 3 Proposed mechanism involving epoxy intermediate for the detection of HOCl by **TVF** moiety.

One of the primary challenges in detecting HOCl in biological systems is the development of highly selective probes that exhibit a distinctive and specific response to HOCl over other reactive oxygen species (ROS), reactive nitrogen species (RNS), and interfering ions. To address this, the selectivity of **TVF** towards HOCl was evaluated in the presence of various common ROS/RNS and selected ions. As shown in Fig. 3, only HOCl triggered a significant enhancement in fluorescence intensity, while other potential interfering species failed to elicit a comparable response. This result highlights the excellent selectivity of the **TVF** probe for HOCl, further supporting its suitability for specific HOCl detection in complex biological environments.

Further, the effect of viscosity on the spectral feature of the **TVF** probe was performed to rule out any possible interference due to the change in viscosity of the medium. Notably, an insignificant change in the fluorescence intensity was observed when the spectra were recorded in a high-viscosity solvent (PEG400) and compared with those recorded in a low-viscosity solvent (methanol) (Fig. S7, ESI†). However, the addition of NaOCl results in a strong emission band, clearly indicating the high selectivity of **TVF** toward HOCl species.

Encouraged by the observation of the solution phase studies of the **TVF** probe, which specifically detects HOCl, we further evaluated its potential for bioimaging. Building on our previous study focusing on mitochondrial targeting for cell tracking,[42] we employed a strategy of labeling cells with probes before subjecting them to any treatments. As our study aims to develop a probe for long-term and real-time detection of HOCl in various physiological conditions, biocompatibility in different types of cells becomes a crucial factor for the success of the probe. As shown in Fig. 4, the **TVF** showed higher cell viability of more than 80% even at higher concentrations of 100 μM for both A549 and L929 cells, indicating excellent biocompatibility in both cells. Hence, the probe can be used for tracking experiments in biological environments.

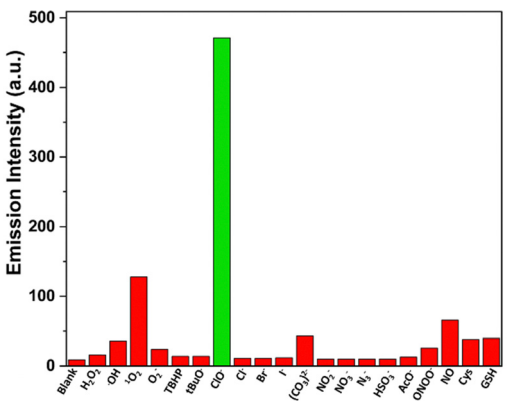

Fig. 3 Fluorescence response of **TVF** (62 μM) toward NaOCl (5 eq.) and other analytes (10 eq.) in methanol. λ_{ex} = 435 nm. Bars represent the fluorescence intensities at 507 nm, and each spectrum was acquired 5 min after HOCl addition.

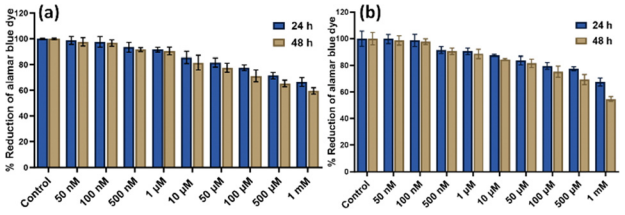

Fig. 4 Biocompatibility of (a) L929 and (b) A549 cells in different concentrations of **TVF** probe (0 nM to 1 mM) was evaluated after 24 h and 48 h.

Next, we further investigated the potential of the **TVF** probe to visualize induced exogenous HOCl production in cancerous and non-cancerous cells. Both the cells showed a feeble fluorescent signal without NaOCl induction (Fig. 5(a) and (b) Control). The weak fluorescent signal in the control cells may be attributed to basal/endogenous HOCl production, which is a characteristic phenomenon in some cells.[44] To eliminate the role of basal HOCl level in sensing exogenous HOCl production, 4-aminobenzoic acid hydrazide (ABAH) was used, which is a potent inhibitor of hypochlorous acid production.[45] Fig. 5 shows that upon ABAH treatment the weak fluorescence signal is significantly reduced as compared to the control cells. This significant decrease in fluorescence intensity upon ABAH treatment indicates the specificity of the probe towards detecting HOCl species over other ROS.[45] Further, when cells were treated with increasing concentrations of NaOCl, a significant increase in fluorescence signal was observed for both cell types, as shown in Fig. 5. This demonstrates the ability of the probe to detect exogenously produced HOCl in a concentration-dependent manner.

Upon successfully imaging exogenous HOCl in cancerous and normal cells, we decided to investigate the potential to monitor endogenous HOCl in macrophages. It is well known that macrophages, as well as other cells of the immune system, can produce endogenous HOCl as a defense mechanism against pathogens like bacteria.[21] RAW 264.7 macrophages are known to produce endogenous HOCl upon induction with bacterial lipopolysaccharide (LPS).[46] It was observed that there was an increase in fluorescence intensity upon an increase in LPS treatment (Fig. 6a), whereas the control cells showed a very weak fluorescence signal (Fig. 6b). To check whether the fluorescence signal is due to the endogenous HOCl species and not due to other ROS, the LPS-treated macrophages were subjected to ABAH treatment. Fig. 6 shows that upon ABAH treatment, fluorescence intensity is significantly reduced compared to both control and LPS treatment groups. This indicates that the **TVF** probe is highly specific in detecting HOCl species in the case of both endogenous and exogenous HOCl production.

Upon successful assessment of endogenous and exogenous HOCl production by the **TVF** probe, we decided to check the subcellular targeting ability of the probe. As the untreated cells showed negligible basal HOCl levels and there was no fluorescence in water, as observed from our solution phase studies (Fig. 1), colocalization experiments were carried out with NaOCl-treated cells. Fig. 7 shows that the green fluorescence from the **TVF** probe overlaid well with the red fluorescence from MitoRed with Pearson colocalization coefficients of 0.95 and 0.88 for L929 and A549 cells, respectively. This indicates the colocalization of the HOCl signal in the mitochondrial region of the cells, proving high mitochondrial targeting ability. In physiological conditions, where cells are organized in three-dimensional structures such as spheroids, a fluorescent probe can be effectively utilized to accurately track and image cells within these complex 3D environments.[47] Furthermore, 3D spheroids more accurately replicate tissue conditions than monolayers and may be more effective for investigating the formation of species such as HOCl, due to enhanced cellular interactions. Fig. 7 shows an appreciable overlay of fluorescence from **TVF** and MitoRed with a Pearson's coefficient of 0.69, indicating colocalization into mitochondria and, hence, proving the appreciable mitochondria targeting ability of the probe in 3D spheroids. A significantly lower overlay and reduced Pearson's colocalization coefficient were observed in spheroids compared to monolayer cells, potentially due to decreased penetration of the probe or MitoRed dye into 3D spheroids relative to monolayer cultures.

Further, we examined the capability of the probe to monitor exogenous HOCl in spheroids. Fig. 8(a) and (b) shows an

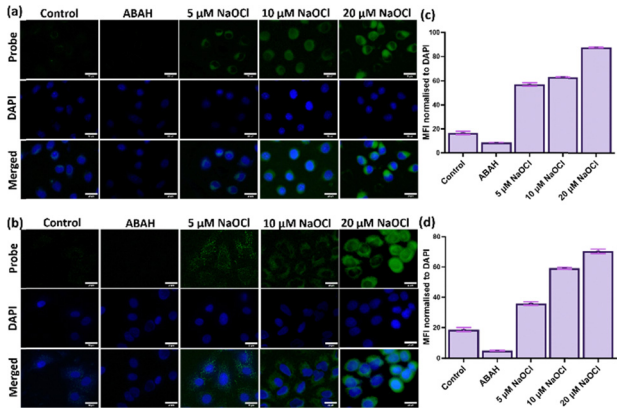

Fig. 5 Tracking exogeneous HOCl production in non-cancerous L929 and cancerous A549 cell lines upon HOCl treatment. (a) L929 and (b) A549 cells pre-tracked with 500 nM of the probe (**TVF**) were treated with ABAH, 5 μM, 10 μM, and 20 μM NaOCl. Quantitative estimation of HOCl production in (c) L929 and (d) A549 cells. Resolution: 100× Scale: 20 μm.

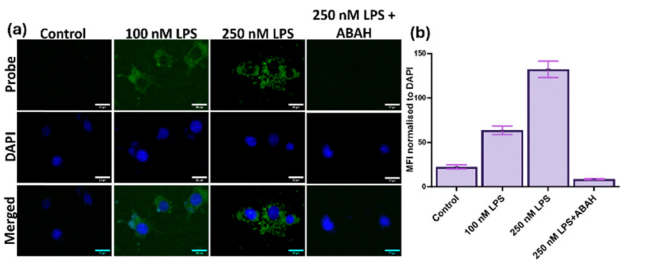

Fig. 6 Tracking endogenous HOCl production in RAW 264.7 macrophages. (a) Macrophages pre-tracked with a 500 nM probe were subjected to 100 nM LPS, 250 nM LPS, and 250 nM LPS + ABAH treatment. (b) Quantitative estimation of HOCl production in RAW 264.7 macrophages upon LPS stimulation. Resolution: 100× Scale: 20 μm.

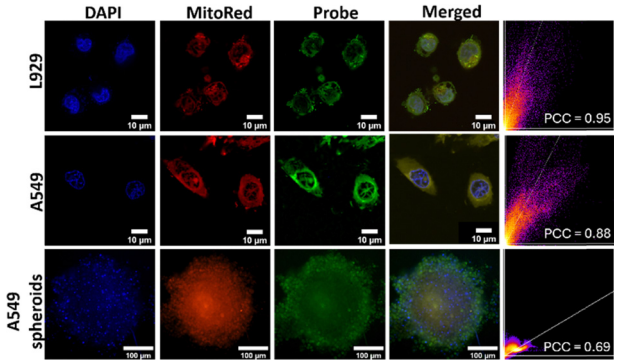

Fig. 7 Mitochondrial colocalization of **TVF** probe. L929 and A549 cells were pretracked with a 500 nM probe (green), followed by NaOCl treatment and staining with 10 nM MitoRed dye (red) and DAPI (blue). Images were captured at 60× resolution. Scale: 10 μm. A549 spheroids pretracked with 500 nM probe (green) and treated with NaOCl, and subsequently co-stained with MitoRed (red) and DAPI. Images were captured at 10× resolution. Scale: 100 μm.

increase in fluorescence signal in a concentration-dependent manner when exposed to NaOCl treatments. Moreover, the control spheroids without any treatment also showed a very weak fluorescence signal, indicating negligible basal HOCl levels, a characteristic of some cancers,[44] which is further reduced upon ABAH treatment. To evaluate the **TVF**'s potential for real-time monitoring of exogenous HOCl production, pre-labeled spheroids were exposed to NaOCl treatment, and fluorescence images were captured at 30-minute intervals over 4 hours. As depicted in Fig. 8(c) and (d), there was a time-dependent increase in fluorescence following NaOCl exposure, demonstrating the probe's capability to detect exogenous HOCl production temporally.

Again, to highlight the importance of the current work in light of the published HOCl probes featuring the HOCl-sensitive olefinic group is summarized in Table S3 (ESI†). Notably, the **TVF** moiety exhibit its high specificity toward HOCl and moderate detection limit, which is suitable for biological applications. Additionally, **TVF** is also found to be effectively labelling the mitochondria. Hence, the **TVF** moiety can be successfully used to monitor intracellular basal HOCl and detect the changes in endogenous and exogenous HOCl in a concentration-dependent and temporal manner within the mitochondria. These observations make, **TVF** a highly relevant probe for studying the oxidative stress conditions.

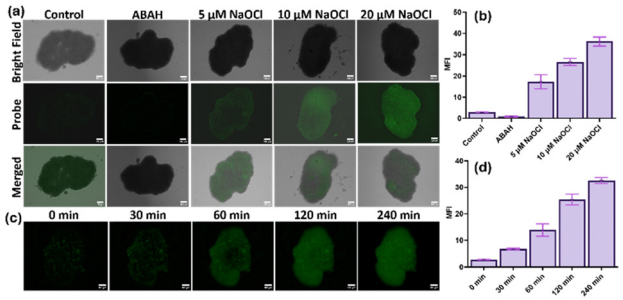

Fig. 8 Real-time monitoring of exogenous HOCl production in A549 spheroids. (a) Probe pretracked A549 spheroids were exposed to varying concentrations of NaOCl, and images were captured at 10× resolution. (b) Quantitative estimation of concentration-dependent HOCl production in A549 spheroids. (c) Pre-tracked A549 spheroids were treated with 5 μM NaOCl and imaged at fixed time intervals (0 min to 240 min). (d) Quantitative estimation of time-dependent HOCl production in A549 spheroids. Resolution: 10× Scale: 10 μm.

Conclusions

In summary, we have designed and synthesized a turn-on fluorescent probe **TVF** to detect HOCl. **TVF** can achieve instantaneous response with a detection limit of 0.36 μM and good selectivity among other analytes. Our study confirms that the **TVF** probe effectively labels live cells and accurately monitors mitochondrial HOCl levels in a concentration-dependent and temporal manner. The high biocompatibility of the **TVF**, even at high concentrations, underscores its suitability for live-cell imaging. Its ability to detect both endogenous and exogenous HOCl in live cells positions it as a valuable tool for developing diagnostic and therapeutic strategies for diseases associated with oxidative stress.

Experimental

Materials and methods

All chemicals and reagents were purchased from commercial sources like Sigma Aldrich, SRL, Alfa Aesar, and TCI chemicals and used without purification. Column chromatography was performed using silica gel (100–200 mesh). Nuclear magnetic resonance spectra were collected using a Bruker DRX-400 spectrometer. ^{13}C NMR spectra were collected at 100 MHz, and ^{1}H NMR spectra were collected at 400 MHz and 600 MHz. Resonances are reported in parts per million (ppm), and coupling constants (J) are reported in hertz (Hz). High-resolution mass spectra (HRMS) were obtained by the electron spray ionization method (ESI) using Agilent QTOF 6538. UV-visible spectral measurements were obtained on a JASCO Spectrophotometer V730, and Fluorescence measurements were taken from JASCO Spectrofluorometer FP-8300. The photophysical studies were performed by adding 5 μL of DMSO stock solution of **TVF** in 3 mL of the respective solvent. Lifetime measurements were performed in Fluoromax-4 Spectrofluorometer (HORIBA Scientific) using a nanoLED-462 for excitation. Various ROS and RNS species are prepared based on the reported literature.[48,49]

Cell culture

A549, L929, and RAW 264.7 cell lines were purchased from NCCS, Pune. Cells were maintained in a DMEM medium containing 10% FBS and 1% penicillin/streptomycin at 37 °C in a CO_2 incubator under 5% CO_2 and 95% humidity. Upon 70% confluency, A549 and L929 cells were sub-cultured by trypsin treatment after subsequent PBS washes. RAW 264.7 macrophages were subcultured by slowly scraping in a cold PBS solution. Seeding density was maintained at 5 × 10^3 cells per cm^2.

Biocompatibility assay

The Alamar Blue cell viability assay was performed per the previously established protocol to check the probe's biocompatibility.[50] A549 and L929 cells were seeded in a 96-well plate at a seeding density of 5×10^3 cells per cm^2. Upon 70% confluency, cells were treated with different concentrations of the probe (50 nM, 100 nM, 500 nM, 1 μM, 10 μM, 50 μM, 100 μM, 500 μM, and 1 mM) in DMEM media. Media was removed after 24 h and 48 h, and 1× Alamar blue dye was added and incubated for 4 hours. After 4 hours, Alamar Blue solution was collected in another plate, and absorbance was measured at 570 nm and 600 nm.

Spheroid formation

A549 spheroids were formed as per the previously established protocol.[51] Briefly, 8×10^3 cells were seeded on 1.5% agarose-coated wells in a 96-well plate and maintained in a CO_2 incubator at 37 °C, 5% CO_2, and 95% humidity. The media was changed every 3 days without disturbing the spheroid.

For the colocalization experiment, cells were visualized using the Nikon AXR system (resonant confocal microscopy), while the EVOS M7000 imaging system (invitrogen) was employed for other tracking experiments.

Tracking cells with TVF probe

After cell splitting, the cell pellet was incubated with a **TVF** probe at a concentration of 500 nM/1×10^6 cells for 15 min and subsequently washed with 1× PBS. Tracked cells were seeded on coverslips at a seeding density of 5×10^3 cells per cm^2 and used for experiments upon reaching 70% confluency. For 3D experiments, tracked cells were seeded on an agarose-coated 96-well plate.

Exogeneous HOCl production and colocalisation with MitoRed dye

Pre-tracked cells on coverslips and spheroids were incubated for 30 minutes with different concentrations of NaOCl (5 μM, 10 μM, and 20 μM) followed by 3 washes with 1× PBS. After PBS washes, cells were counterstained with DAPI (1 μg mL^{-1}) for 5 minutes. Fluorescent images were captured under 100× oil immersion objective in green channel (λ_{ex} = 488 nm, λ_{em} = 500–580 nm) and blue channel (λ_{ex} = 405 nm, λ_{em} = 440–480 nm). To eliminate the appearance of fluorescence signal due to basal HOCl, cells were treated with 200 μM ABAH. Mean fluorescence intensity (MFI)/DAPI ratio was calculated using ImageJ.

For colocalization, pre-tracked cells and spheroids were treated with 20 μM NaOCl and incubated with 10 nM MitoRed dye for 30 min at 37 °C. Cells were counterstained with DAPI (1 μg mL^{-1}), and images were captured under 100× oil immersion objective in the green channel (λ_{ex} = 488 nm, λ_{em} = 500–580 nm), blue channel (λ_{ex} = 405 nm, λ_{em} = 440–480 nm) and red channel (λ_{ex} = 540 nm, λ_{em} = 580–620 nm). Colocalization analysis was performed using ImageJ.

Endogenous HOCl production

Pre-tracked RAW 264.7 macrophages were incubated with 100 nM and 250 nM LPS for 6 hours. After incubation, coverslips were washed thrice with 1× PBS. Cells were counterstained with DAPI (1 μg mL^{-1}) for 5 minutes. Fluorescent images were captured under 100× oil immersion objective in green channel (λ_{ex} = 488 nm, λ_{em} = 500–580 nm) and blue channel (λ_{ex} = 405 nm, λ_{em} = 440–480 nm). Mean fluorescence intensity (MFI)/DAPI ratio was calculated using ImageJ.[50]

Synthetic procedures

The procedure for the synthesis of **1** and **2** has been reported previously.[52,53]

Synthesis of compound 3

Compounds **1** (0.5 g, 1.9 mmol) and **2** (0.57 g, 2.1 mmol) were dissolved in dry DMF (8 mL) and placed into a predried seal tube. Further, triethylamine (0.6 mL), tri-*o*-tolyl phosphine (0.09 g, 0.29 mmol), and $Pd(OAc)_2$ (0.02 g, 0.09 mmol) were added to the reaction mixture. The resulting solution was degassed under nitrogen and heated up to 120 °C for 24 h. After cooling to room temperature, the reaction mixture was separated by chloroform/water mixture to obtain crude compounds, which were then further purified by column chromatography (v/v hexane–chloroform (9/1)). Pure compound **3** was obtained as a reddish-brown powder. (Yield: 48%).

^{1}H NMR (400 MHz, $CDCl_3$): δ 8.23 (d, J = 2.1 Hz, 1H), 8.17 (t, J = 5.1 Hz, 1H), 7.62 (dd, J = 9.0, 2.1 Hz, 1H), 7.37–7.31 (m, 2H), 7.28–7.21 (m, 4H), 7.13–7.00 (m, 8H), 6.87 (dd, J = 16.3, 9.0 Hz, 3H), 3.30 (td, J = 7.1, 5.4 Hz, 2H), 1.97–1.64 (m, 2H), 1.06 (t, J = 7.4 Hz, 3H).^{13}C NMR {^{1}H} (101 MHz, $CDCl_3$): δ 147.62, 147.36, 144.98, 133.90, 131.64, 131.39, 129.40, 127.22, 126.70, 125.54, 124.97, 124.59, 124.43, 123.69, 123.15, 114.35, 45.00, 22.42, 11.71 ppm. HRMS (ESI) m/z: $[M + H]^+$ calcd for **3** : 450.2176 Found 450.2175.

Synthesis of compounds TVF

The compound **3** (0.4 g, 0.9 mmol) was dissolved in MeOH (15 mL) and heated at 80 °C. Further, Pd/C (0.05 g) was added into the solution, followed by a gradual addition of 1 g of 85% hydrazine hydrate for about 0.5 h, and the reaction was monitored through TLC. After completion of the reaction, Pd/C was removed by vacuum filtration using chloroform, and the filtrate was concentrated under vacuum to give the crude product. Then, alloxan monohydrate (0.14 g, 0.9 mmol) and boric acid (0.05 g, 0.9 mmol) were added in a round-bottom flask and dissolved in methanol (8 mL). Acetic acid solution (24 mL) of crude product was slowly added to the reaction mixture and stirred under an inert atmosphere overnight at room temperature. Diethyl ether was added to the reaction mixture, followed by stirring for 1 h to yield a crude precipitate, which was filtered by vacuum filtration using water and diethyl ether. The crude solid was further purified by column chromatography on silica gel using chloroform/methanol as eluent. Pure compound **TVF** was obtained as a dark purple solid (yield: 25%).

^{1}H NMR (400 MHz, DMSO-d_6) δ 11.39 (s, 1H), 8.23 (s, 1H), 8.18 (d, J = 9.0 Hz, 1H), 7.98 (d, J = 9.1 Hz, 1H), 7.56 (d, J = 8.5 Hz, 2H), 7.44 (d, J = 16.4 Hz, 1H), 7.35–7.28 (m, 5H), 7.07 (dd, J = 15.6, 7.6 Hz, 6H), 6.97 (d, J = 8.5 Hz, 2H), 4.55 (t, J = 8 Hz, 2H),

1.76 (dd, J = 15.1, 7.5 Hz, 2H), 1.03 (t, J = 7.4 Hz, 3H). $^{13}C\{^{1}H\}$ NMR (75 MHz, DMSO-d_6): δ 159.86, 155.77, 150.08, 147.27, 146.94, 138.94, 135.50, 132.78, 131.66, 130.85, 130.15, 129.74, 128.37, 128.04, 124.41, 123.56, 122.74, 116.86, 45.80, 20.05, 11.08 ppm. HRMS (ESI) m/z: [M + H]+ calcd for **TVF**: 526.2238 found 526.2230.

Data availability

The data supporting this article have been included as part of the ESI.† Note: the same has been applied for patent as mentioned in the conflict of interest section.

Conflicts of interest

This work including synthesis and other details has been filed for patent with application number 202441085937. All the authors of this manuscript are the applicants.

Acknowledgements

AKM thanks Science and Engineering Research Boards (SERB) India for the (CRG/2022/006706). All authors thank the Indian Institute of Technology (IIT)-Hyderabad for providing infrastructure and instrument facilities. We thank centre for *In situ* and Correlative Microscopy (SATHI-CISCoM) at IIT-Hyderabad for providing access to confocal microscopy imaging facility.

References

1 P. Gao, W. Pan, N. Li and B. Tang, *Chem. Sci.*, 2019, **10**, 6035–6071.
2 J. Kay, E. Thadhani, L. Samson and B. Engelward, *DNA Repair*, 2019, **83**, 102673.
3 M. H. Lee, N. Park, C. Yi, J. H. Han, J. H. Hong, K. P. Kim, D. H. Kang, J. L. Sessler, C. Kang and J. S. Kim, *J. Am. Chem. Soc.*, 2014, **136**, 14136–14142.
4 K. Zhou, Y. Wang, X. Huang, K. Luby-Phelps, B. D. Sumer and J. Gao, *Angew. Chem., Int. Ed.*, 2011, **50**, 6109–6114.
5 Q. Wan, S. Chen, W. Shi, L. Li and H. Ma, *Angew. Chem., Int. Ed.*, 2014, **53**, 10916–10920.
6 N. Jiang, J. Fan, F. Xu, X. Peng, H. Mu, J. Wang and X. Xiong, *Angew. Chem., Int. Ed.*, 2015, **54**, 2510–2514.
7 P. Chabosseau, E. Tuncay, G. Meur, E. A. Bellomo, A. Hessels, S. Hughes, P. R. V. Johnson, M. Bugliani, P. Marchetti, B. Turan, A. R. Lyon, M. Merkx and G. A. Rutter, *ACS Chem. Biol.*, 2014, **9**, 2111–2120.
8 Y. Han, C. Ding, J. Zhou and Y. Tian, *Anal. Chem.*, 2015, **87**, 5333–5339.
9 Z. Yang, Y. He, J.-H. Lee, N. Park, M. Suh, W.-S. Chae, J. Cao, X. Peng, H. Jung, C. Kang and J. S. Kim, *J. Am. Chem. Soc.*, 2013, **135**, 9181–9185.
10 D. Li, X. Tian, A. Wang, L. Guan, J. Zheng, F. Li, S. Li, H. Zhou, J. Wu and Y. Tian, *Chem. Sci.*, 2016, **7**, 2257–2263.
11 L. M. Hyman and K. J. Franz, *Coord. Chem. Rev.*, 2012, **256**, 2333–2356.
12 X. Jiang, L. Wang, S. L. Carroll, J. Chen, M. C. Wang and J. Wang, *Antioxid. Redox Signaling*, 2018, **29**, 518–540.
13 X. Chen, F. Wang, J. Y. Hyun, T. Wei, J. Qiang, X. Ren, I. Shin and J. Yoon, *Chem. Soc. Rev.*, 2016, **45**, 2976–3016.
14 V. S. Lin, A. R. Lippert and C. J. Chang, *Proc. Natl. Acad. Sci. U. S. A.*, 2013, **110**, 7131–7135.
15 F. Yang, H. Gao, S.-S. Li, R.-B. An, X.-Y. Sun, B. Kang, J.-J. Xu and H.-Y. Chen, *Chem. Sci.*, 2018, **9**, 5556–5563.
16 X. Yang, Y. Zhou, X. Zhang, S. Yang, Y. Chen, J. Guo, X. Li, Z. Qing and R. Yang, *Chem. Commun.*, 2016, **52**, 10289–10292.
17 J. Ning, Z. Lin, X. Zhao, B. Zhao and J. Miao, *Cell Death Dis.*, 2019, **10**, 858.
18 D. Roos and C. C. Winterbourn, *Science*, 2002, **296**, 669–671.
19 F. C. Fang, *Nat. Rev. Microbiol.*, 2004, **2**, 820–832.
20 A. Strzepa, K. A. Pritchard and B. N. Dittel, *Cell. Immunol.*, 2017, **317**, 1–8.
21 Z. M. Prokopowicz, F. Arce, R. Biedron, C. L.-L. Chiang, M. Ciszek, D. R. Katz, M. Nowakowska, S. Zapotoczny, J. Marcinkiewicz and B. M. Chain, *J. Immunol.*, 2010, **184**, 824–835.
22 M. Ren, K. Zhou, L. He and W. Lin, *J. Mater. Chem. B*, 2018, **6**, 1716–1733.
23 P. Nahon, A. Sutton, P. Rufat, M. Ziol, H. Akouche, C. Laguillier, N. Charnaux, N. Ganne-Carrié, V. Grando-Lemaire and G. N'Kontchou, *Hepatology*, 2009, **50**, 1484–1493.
24 P. Palladino, F. Torrini, S. Scarano and M. Minunni, *J. Pharm. Biomed. Anal.*, 2020, **179**, 113016.
25 H. Jaeschke and A. Ramachandran, *J. Hepatol.*, 2011, **55**, 227.
26 D. Wu, L. Chen, Q. Xu, X. Chen and J. Yoon, *Acc. Chem. Res.*, 2019, **52**, 2158.
27 N. Kwon, Y. Chen, X. Chen, M. H. Kim and J. Yoon, *Dyes Pigm.*, 2022, **200**, 110132.
28 Y. Fang and W. Dehaen, *Molecules*, 2021, **26**, 363.
29 M. Ren, K. Zhou, L. He and W. Lin, *J. Mat. Chem. B*, 2018, **6**, 1716.
30 Y.-R. Zhang, Y. Liu, X. Feng and B.-X. Zhao, *Sens. Actuators, B*, 2017, **240**, 18.
31 A. Kaur and E. J. New, *Acc. Chem. Res.*, 2019, **52**, 623–632.
32 D. Mondal, I. Naskar, M. Deepa and A. K. Mishra, *Energy Adv.*, 2024, **3**, 1710–1716.
33 M. V. Mouli and A. K. Mishra, *CrystEngComm*, 2022, **24**, 2221–2225.
34 M. V. Mouli and A. K. Mishra, *Org. Biomol. Chem.*, 2023, **21**, 5622–5628.
35 M. V. Mouli and A. K. Mishra, *Dyes Pigm.*, 2023, **212**, 111148.
36 M. V. Mouli, S. Katyal and A. K. Mishra, *Synlett*, 2023, 829–834.
37 M. V. Mouli, D. Mondal, K. Kumari, S. K. Singh and A. K. Mishra, *Org. Biomol. Chem.*, 2023, **21**, 3311–3316.
38 H. G. Agrawal, A. Dubey, D. Mondal and A. K. Mishra, *Chem. – Asian J.*, 2025, **20**, e202401099.
39 H. G. Agrawal, S. Raha and A. K. Mishra, *J. Mol. Struct.*, 2025, **1319**, 139229.
40 H. G. Agrawal, S. Khatun, A. K. Rengan and A. K. Mishra, *Polyhedron*, 2023, **243**, 116536.
41 M. V. Mouli and A. K. Mishra, *Org. Biomol. Chem.*, 2023, **21**, 5622–5628.

42 H. G. Agrawal, P. S. Giri, P. Meena, S. N. Rath and A. K. Mishra, *ACS Med. Chem. Lett.*, 2023, **14**, 1857–1862.
43 M. Li, J. Chao, Y. Liu, M. Xu, Y. Zhang, F. Huo, J. Wang and C. Yin, *Spectrochim. Acta, Part A*, 2020, **229**, 118001.
44 L. Wang, J. Liu, H. Zhang and W. Guo, *Sens. Actuators, B*, 2021, **334**, 129602.
45 A. J. Kettle, C. A. Gedye and C. C. Winterbourn, *Biochem. J.*, 1997, **321**, 503–508.
46 P. Luo and X. Zhao, *ACS Omega*, 2021, **6**, 12287–12292.
47 C. Jubelin, J. Muñoz-Garcia, L. Griscom, D. Cochonneau, E. Ollivier, M.-F. Heymann, F. M. Vallette, L. Oliver and D. Heymann, *Cell Biosci.*, 2022, **12**, 155.
48 Y. He, T. Yang, B. Lin, J. Fan and Y. Han, *New J. Chem.*, 2024, **48**, 8809–8817.
49 W. Zhao, S. Zhang, J. Yan, P. Xu, B. Li, Y. Zhang, J. Li and S. Wu, *Sens. Actuators, B*, 2024, **412**, 135813.
50 P. S. Giri and S. N. Rath, *ACS Appl. Bio Mater.*, 2024, **7**, 2413–2422.
51 V. S. Sukanya, P. S. Giri, V. Nellore and S. N. Rath, *Biomater. Sci.*, 2023, **11**, 4265–4280.
52 S.-L. Deng, T.-L. Chen, W.-L. Chien and J.-L. Hong, *J. Mater. Chem. C*, 2014, **2**, 651–659.
53 H. G. Agrawal, S. Khatun, A. K. Rengan and A. K. Mishra, *Chem. – Eur. J.*, 2024, **30**, e202401483.